In vivo identification of ribonucleoprotein–RNA interactions

Jennifer Zielinski*†, Kalle Kilk†‡, Tiina Peritz*, Theresa Kannanayakal*, Kevin Y. Miyashiro*, Emelía Eiríksdóttir‡, Jeanine Jochems*, Ülo Langel‡, and James Eberwine*§

*Department of Pharmacology, University of Pennsylvania School of Medicine, Philadelphia, PA 19104; and ‡Department of Neurochemistry and Neurotoxicology, Stockholm University, SE-106 91 Stockholm, Sweden

Communicated by William T. Greenough, University of Illinois, Urbana, IL, December 9, 2005 (received for review September 27, 2005)

To understand the role of RNA-binding proteins (RBPs) in the regulation of gene expression, methods are needed for the *in vivo* identification of RNA–protein interactions. We have developed the peptide nucleic acid (PNA)-assisted identification of RBP technology to enable the identification of proteins that complex with a target RNA *in vivo*. Specific regions of the 3′ and 5′ UTRs of *ankylosis* mRNA were targeted by antisense PNAs transported into cortical neurons by the cell-penetrating peptide transportan 10. An array of proteins was isolated in complex with or near the targeted regions of the *ankylosis* mRNA through UV-induced crosslinking of the annealed PNA–RNA–RBP complex. The first evidence for pharmacological modulation of these specific protein–RNA associations was observed. These data show that the PNA-assisted identification of the RBP technique is a reliable method to rapidly identify proteins interacting *in vivo* with the target RNA.

RNA-binding proteins

Numerous cellular events, including premRNA splicing, mRNA editing, export of the mRNA from the nucleus to the cytoplasm, and the stability and translational control of mRNAs, provide opportunities to regulate gene expression at the RNA level. RNA-binding proteins (RBPs) are crucial functional components of the molecular machineries involved in each of these posttranscriptional events (1). Disruption of RBP activity has been implicated in the pathogenesis of epilepsy (2), rheumatism (3), cancer (2), motor neuron disease (4), and mental retardation (5).

Traditionally, *in vitro* methodologies are used to understand RNA–RBP interactions, and these methods generally use one of two approaches. First, a known RBP can be targeted to identify RNAs that may interact with it. Conventional gel-shift or supershift assays, for example, are commonly used to assess RBP activity by showing that RNA migration in PAGE is retarded after incubation with protein in the presence or absence of an antibody recognizing an epitope on the protein. The second approach involves identification of any RBP associated with the target RNA; this can be achieved by binding an antisense oligonucleotide to a matrix through which a cell lysate will be passed in hopes of binding the target RNA and its associated proteins. Intrinsic to these methodologies are the limitations in their ability to provide a complete picture of RBP activity because they show only what binding occurs *in vitro*, often under nonphysiological conditions. To truly understand the dynamics of RNA–RBP interactions, it is necessary to identify the interactions *in vivo*. Although several procedures, such as RBP immunoprecipitation (IP) (6, 7), crosslinking immunoprecipitation (8), and antibody-positioned RNA amplification (9), permit the characterization of RNA cargoes that bind to a previously identified RBP, few methodologies exist to faithfully characterize the panoply of RBPs that bind to any particular RNA under a defined set of physiological stimuli.

Here we describe the peptide nucleic acid (PNA)-assisted identification of RBPs (PAIR) methodology that provides for the *in vivo* identification of the RBPs that interact with a specific target mRNA sequence. This is accomplished through a PNA coupled to a cell-penetrating peptide (CPP) as well as a photoactivatable compound. PNAs are nucleic acid analogs in which the sugar–phosphate backbone is replaced by a polyamide skeleton without altering the position of nucleobases (10, 11). The PNA binds RNA with high specificity and selectivity, and the PNA–RNA hybrids are more stable and form faster (11), with increased specificity (12), than the corresponding nucleic acid hybrids. These characteristics, in combination with their resistance to proteases and nucleases (13), have permitted PNAs to be used in various molecular biological (11, 14–16) as well as therapeutic contexts (17–20). However, PNA oligomers are not readily internalized in intact cells. An efficient strategy for the delivery of bioactive compounds into living cells is the use of CPPs. The CPP transportan can cross the extracellular lipid bilayer (21) and facilitate the translocation of proteins, small molecules (22), and PNA antisense oligomers as cargoes (23). Transportan 10 (TP10), used in this study, is a truncated analogue of the full-length transportan protein lacking the GTPase activity found in the native sequence (24).

We have used *ankylosis* (*ank*) RNA (GenBank accession no. AF393241), a panneuronal dendritically localized RNA, in the development of PAIR. The ank protein has been described as an inorganic pyrophosphate transporter (25). The dendritic localization of RNAs is a rare event occurring for only ≈5% of the cellular RNAs (26). Given the importance of the ank protein in the periphery, as well as the distinct neuronal subcellular localization, it is anticipated that the identification of RBPs that complex with the *ank* mRNA may provide insight into these biological phenomena.

We used TP10 for the intracellular delivery of PNA oligomers that bind to *ank* mRNA. Attached to the PNA is *p*-benzoylphenylalanine (Bpa), a photoactivatable amino acid adduct (Fig. 1). After transport into the cell, the disulfide bond between the CPP and PNA is reduced (22), and the PNA will hybridize to its complementary *ank* mRNA target. Subsequently administered UV irradiation will release the benzoyl moiety of the Bpa, creating a free phenylalanine radical able to crosslink the nearest molecules (i.e., the RBPs). The PNA–ribonucleotide complex is isolated by hybridization of a biotinylated sense (antisense to PNA) oligonucleotide coupled to streptavidin magnetic beads (schematized in Fig. 1*A*). This PNA-assisted identification of RBPs provides an *in vivo* methodology through which RBPs interacting with any target mRNA can be identified.

Results

Development of the PAIR Technology. To show that *ank* PNAs can localize in live cortical neurons within 90 min, an Oregon green

Conflict of interest statement: No conflicts declared.

Freely available online through the PNAS open access option.

Abbreviations: PNA, peptide nucleic acid; RBP, RNA-binding protein; PAIR, PNA-assisted identification of RBPs; TP10, transportan 10; ARE, AU-rich elements; IP, immunoprecipitation; NB, neurobasal; NB/B27, NB with B27 supplement; CPP, cell-penetrating peptide; Bpa, *p*-benzoylphenylalanine; *ank*, *ankylosis*; hnRNP, heteronuclear ribonucleoprotein; DHPG, (*S*)-3,5-dihydroxphenylglycine; ISH, *in situ* hybridization.

†J.Z. and K.K. contributed equally to this work.

§To whom correspondence should be addressed. E-mail: eberwine@mail.med.upenn.edu.

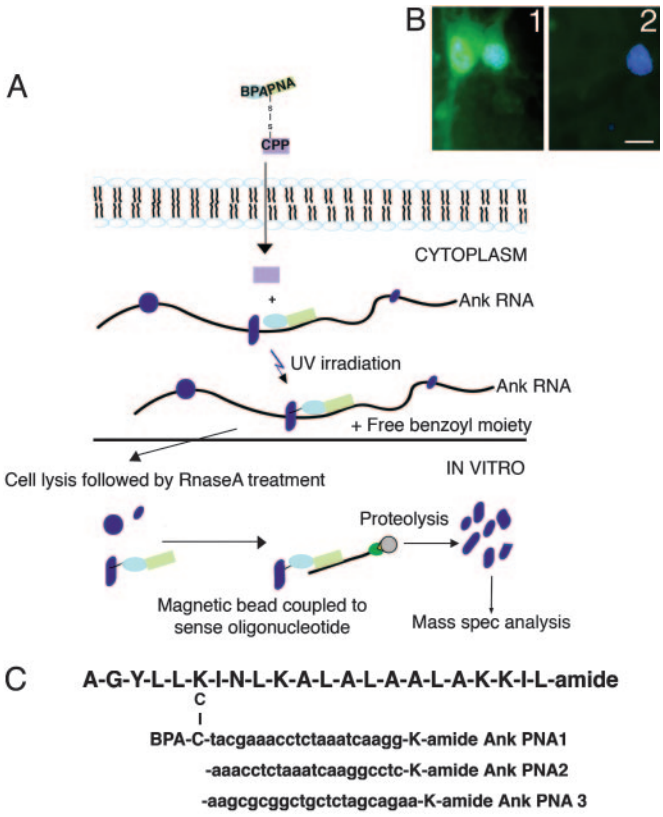

Fig. 1. Schematic of the PAIR technology; PNA structure and intracellular delivery. (*A*) After entry into the cell, the BPA–PNA will dissociate from the CPP. The PNA will hybridize to its complementary sequence positioning the photoactivatible BPA in proximity to the target RNA. UV irradiation will crosslink the nearest substances, i.e., RBPs, with the PNA. After cell lysis and RNase treatment, the PNA–RBP complexes are isolated by using magnetic beads coupled to a sense oligo. The isolated material is proteolyzed and analyzed by mass spectrometry. (*B1*) An Oregon green 488-labeled sense oligonucleotide was annealed to the *ank* PNA 1; this fluorescently labeled PNA–DNA hybrid was incubated with cortical neurons and its intracellular localization visualized by fluorescence microscopy. (*B2*) The lack of signal when the fluorescent oligonucleotide was incubated with the cells without PNA. (Scale bar, 20 μm.) (*C*) The CPP and BPA portion is the same in *ank* PNAs 1, 2, and 3; the PNA sequence varies. The numbers 1, 2, 3 refer to the complementary *ank* mRNA sequence (GenBank accession no. AF393241).

488-labeled antisense oligonucleotide was annealed *in vitro* to *ank* PNA 1. *ank* PNA 1-oligo-fluorophore was incubated with the cells. Fig. 1*B* shows that the PNA–fluorophore complex is translocated into the cell by the TP10, as illustrated by fluorescence throughout the cell soma and dendrites and in some nuclei.

In our optimized experimental paradigm, the PNA (structures shown in Fig. 1*C*) was incubated with cells at a final concentration of 50 nM in neurobasal (NB) with B27 supplement (NB/B27) for 90 min and UV-irradiated for 2.5 min, followed by cell lysis in Triton X-100 lysis buffer. These conditions repeatedly yielded the most consistent binding patterns while minimizing nonspecific binding (Fig. 2). There are no bound proteins observed in the absence of *ank* PNA 1 (Fig. 2, lane A), UV (Fig. 2, lane B), or both (Fig. 2, lane C). Bound proteins of various molecular weights are visualized with the use of 50 nM *ank* PNA 1 and subsequent UV irradiation (Fig. 2, lane D). The specificity of the binding is illustrated by the different binding patterns when using a distinct PNA-targeting GluR2 (Fig. 2, lane E). This control is superior to a sense or mixed PNA, because a PNA that binds to an endogenous RNA and shows a different pattern proves that the interactions are sequence-specific and not random protein binding to the PNA. In both the

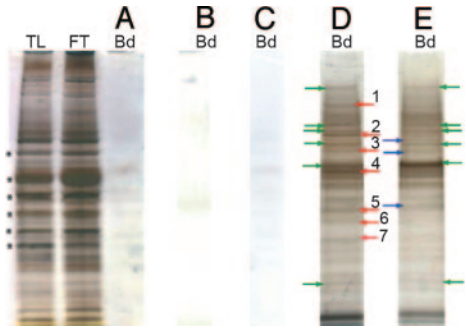

Fig. 2. Specificity of PAIR Isolation of *ank* mRBPs. Silver staining of total lysate (TL), DNA–column flowthrough (FT), and PNA–DNA column-bound (Bd) proteins for each of the following conditions: (lane A) no PNA was added, but the neurons were UV-irradiated for 2.5 min; (lane B) 50 nM *ank* PNA 1 was added to the cells; no UV irradiation; (lane C) no PNA, no UV; (lane D) the complete PAIR protocol: 50 nM *ank* PNA 1 for 90 min, 2.5-min UV irradiation and cell lysis, and (lane E) incubation with a PNA against GluR2 mRNA followed by the complete PAIR protocol. High-abundance bands seen in total lysate and FT (marked by asterisks in lane A) are not apparent in the bound lysates. Distinct bands are enriched by the PAIR protocol, as seen in lanes D (*ank* PNA 1) and E (GluR2 PNA). Arrows between lanes D and E point to the differences between proteins bound by *ank* PNA 1 (red arrows) and GluR2 PNA (blue arrows), respectively. The numbered red arrows correspond to the following proteins: 1, nucleolin; 2, hnRNP L; 3, hnRNP K; 4, hnRNP X; 5, hnRNP C1/C2; 6, hnRNP A1; and 7, hnRNP A2/B1. The green arrows indicate protein bands of the same apparent molecular weight.

total lysate and the flowthrough (FT), there are numerous high-abundance protein bands (asterisks in Fig. 2) that are not seen in the bound fractions. Instead, distinct bands are enriched by the PAIR protocol, as seen in Fig. 2, lanes D (*ank* PNA) and E (GluR2 PNA). The arrows between Fig. 2, lanes D and E, point to the differences between the proteins bound by *ank* PNA 1 (red arrows) and GluR2 PNA (blue arrows). The green arrows on the periphery indicate bands of the same molecular weight. Protein sequences corresponding to these bands are determined by mass spectrometry once the bands have been extracted from the gel. Differences are evident in the intensity of the bands, as seen in the relatively low number of proteins that are captured in the bound portion of the lysate in comparison with the numerous high-abundance bands in the total lysate and the FT.

In previous studies, the distance between moieties that are to be UV-crosslinked has been shown to be ≈4.5 Å (27) or less; consequently, the PAIR-isolated RBPs should be no more than 4.5 Å from the photoactivatable Bpa. This short distance, coupled with the repeated isolation of multiple proteins, strongly supports the notion that there is a direct interaction of these isolated RBPs with the *ank* mRNA.

Proteins Identified in Complex with *ank* mRNA Using PAIR. Protein bands were excised from SDS/PAGE gels and digested with trypsin followed by mass spectrometry; mass spectrometry analysis results in identification of proteins with differing levels of confidence. Confidence levels are increased when multiple peptides from the same protein are identified or when masses can be unambiguously assigned to specific peptide fragments. The RBPs we have found interacting with *ank* RNA (>95% confidence) are shown in Fig. 3, which summarizes the RBPs that bound to each of the three distinct *ank* PNAs after differing pharmacological challenges.

Among the RBPs that were isolated, nucleolin was identified under all physiological conditions and with each of the three PNAs (Fig. 3). This is not surprising, because *ank* mRNA contains two nucleolin-binding sequences. Other isolated RBPs interacted with *ank* mRNA only under distinct physiological conditions or in a region-specific manner. Heteronuclear ribonucleoprotein

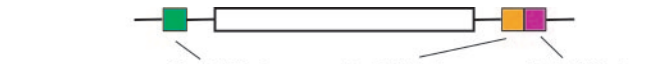

	Ank PNA 3	Ank PNA 2	Ank PNA 1
Basal	Nucleolin (4/6)	Nucleolin (4/4)	Nucleolin (5/6)
	hnRNP U (3/6)	hnRNP U (4/4)	
	TAR (2/6)	TAR (2/4)	
		hnRNP A2/B1 (3/4)	hnRNP A2/B1 (1/6)
	hnRNP C1/C2 (4/6)	hnRNP C1/C2 (1/4)	
			hnRNP K (2/6)
	hnRNP G (1/6)	hnRNP G (1/4)	
		hnRNP A3 (1/4)	
		hnRNP R (1/4)	
		Splicing Prp8 (1/4)	
			hnRNP A1 (1/6)
			hnRNP L (1/6)
	U5 snRNP (1/6)		
BDNF	Nucleolin (4/4)	Nucleolin (4/4)	Nucleolin (5/6)
	hnRNP C1/C2 (3/4)	hnRNP C1/C2 (3/4)	
		hnRNP A1 (1/4)	hnRNP A1 (4/6)
			hnRNP A2/B1 (3/6)
	hnRNP G (3/4)	hnRNP G (3/4)	
	hnRNP U (3/4)	hnRNP U (3/4)	
	AUF 1 (2/4)	AUF 1 (2/4)	AUF 1 (1/6)
		Ribo Prot L22 (3/4)	Ribo Prot L22 (1/6)
		Ribo Prot L23a (4/4)	Ribo Prot L23a (6/6)
		Ribo Prot L25 (4/4)	Ribo Prot L25 (6/6)
			Fus (pigpen) (3/6)
			hnRNP A3 (2/6)
			hnRNP L (2/6)
			hnRNP K (2/6)
			SAP 145 (2/6)
			PTB-Assoc. Splicing (2/6)
			mRNA Splicing 75 (1/6)
K+	Nucleolin (4/4)	Nucleolin (3/4)	Nucleolin (4/4)
	U5 snRNP (2/4)		
		hnRNP G (2/4)	
			hnRNP K (2/6)
DHPG	Nucleolin (4/4)	Nucleolin (2/4)	Nucleolin (4/4)
	hnRNP D (2/4)		hnRNP D (2/4)
	Cold-Induced RBP (2/4)		
			hnRNP K (3/4)

Fig. 3. Pharmacological regulation of the association of RBPs with *ank* mRNA. Pharmacological manipulations of the primary rat cortical cells consisted of 20 mM DHPG for 30 min, 3 mM K^+ for 5 min, or 50 ng/ml BDNF for 3 h. The numbers in parentheses refer to the number of times the RBP was detected (numerator) versus the number of times the experiments were performed (denominator).

(hnRNP) U, for example, was found to associate with *ank* mRNA in the regions of *ank* PNA 2 and 3. Another hnRNP family member, hnRNP K, on the other hand, is found to complex solely with *ank* PNA 1 in one-third of the experiments. hnRNP A2 was found to complex with only the 3′ UTR associating with *ank* PNA 2. Interestingly, hnRNP A2 has been identified as a 40S core particle often found in complex with hnRNP A1, B1, C1, and C2, among others (28). These core particles are known to bind nascent RNA and function in its maturation and in the stability of the transcript (29, 30).

In an effort to determine whether RNA-binding activity changes in response to the known modulator of translation, we characterized the RBPs associated with *ank* mRNA after BDNF stimulation. AUF1 was found in association with *ank* mRNA only after BDNF treatment, not under basal conditions; this association was detected with all three PNAs. Other BDNF-triggered RBP associations were PNA specific. Fus (pigpen) RBP associated with *ank* mRNA only in the region of PNA 1. In addition, the association of hnRNP A1 with *ank* mRNA increased in frequency when BDNF treated as indicated by RBP isolation in four of six trials, as opposed to one of six for pharmacologically naive cells. The effect that BDNF stimulation has on *ank* mRNA interaction(s) with hnRNP A2/B1 is complex. In response to BDNF, this association was detected with increased frequency with *ank* PNA 1, but the treatment hinders the interaction detectable by *ank* PNA 2. hnRNP U is isolated in complex with both PNA 2 and 3. This interaction is detectable under basal and BDNF-stimulated conditions but not after (*S*)-3, 5-dihydroxyphonylglycine (DHPG) [a metabotropic glutamate receptor agonist known to stimulate dendritic protein synthesis (31, 32)] or high potassium (K^+) treatment [which induces depolarization and activity-dependent protein synthesis (33)]. Observed to function in cytoplasmic trafficking of RNA (30), hnRNP A3 is shown to interact with the 3′ UTR of *ank* mRNA, isolated with *ank* PNA 2 under basal conditions, and with *ank* PNA 1 after BDNF stimulation. These data reinforce the notion that RNA–RBP interactions are dynamic processes involving remodeling of the mRNP in response to external stimuli.

IP of mRNA–Protein Complexes. IP of RNA–protein complexes (6) was used to confirm results obtained with the PAIR technology (Fig. 4*A*). Two of the proteins found to bind to *ank* mRNA, nucleolin (lane 2) and hnRNP K (lane 3), were immunoprecipitated from a lysate of cultured rat cortical neurons, and RT-PCR was performed on the immunoprecipitated material by using *ank*-specific primers. An anti-GFP antibody (lane 4), as well as protein A beads without antibody (lane 5), was used as negative control. After a first round of PCR, nested PCR resulted in PCR products of the correct size in the corresponding nucleolin and hnRNP K lanes but not in the negative control lanes. This shows that *ank* mRNA coprecipitated with both nucleolin and hnRNP K. The absence of the PCR product in negative controls indicated that the association of nucleolin and hnRNP K proteins with the *ank*–mRNA complex was specific.

Immunocytochemistry, RNA Granule Staining, and *in Situ* Hybridization (ISH). *ank* mRNA was visualized by ISH by using a fluorescently labeled antisense probe in fixed rat cortical neurons (Fig. 4*B*, red). The association of *ank* mRNA with RNA granules was assessed by using Syto-14 granule stain (Fig. 4*Ba*, green) (34). Colocalization of Syto-14 staining (Fig. 4*Ba*, green arrow) with *ank* mRNA (red arrow) is observed as yellow (yellow arrow). The overlap of fluorescent signals reveals *ank* mRNA coexists with RNA granules. Nucleolin, hnRNP K, and hnRPN U were repeatedly identified in complex with *ank* RNA, hence these RBPs were chosen as representatives to immunocytochemically visualize the *ank* mRNA colocalization with the PAIR-identified RBPs. Fig. 4 *Bb* (hnRNP U), *Bc* (hnRNP K), and *Bd* (nucleolin) show the immunocytochemical staining of individual RBPs (green), coincident with *ank* mRNA (red), with the color overlap visible as yellow. The magnified insets from each of the RBP-*ank* colocalization studies (Fig. 4 *Bb–Bd Insets*) illustrate the heterogeneity of RBP association with RNAs, because a fraction of the individual RBPs are visible with little or no overlap with *ank* mRNA (green arrows), *ank* mRNA can exist with little or no overlap with the designated RBP (red arrows), and a large fraction of both exhibit the yellow overlap (yellow arrows) indicative of colocalization.

Discussion

Knowledge of RBPs is essential for understanding the complexities of gene expression. To advance this knowledge, we have developed the PAIR technology by using *ank* RNA to identify the RBPs *in vivo*. Before the present studies, no RBPs had been identified as binding to *ank* RNA. The identification of these proteins will permit detailed analysis of aspects of *ank* mRNA localization and translation. Using PNAs against the 5′ and 3′ UTR regions, we found that a larger number of proteins associate with the 3′ than the 5′ UTR region (Fig. 3), as predicted in the literature. Further differential binding of RBPs to PNA1 and PNA2 could be due to a direct but distinct interaction of the protein with both mRNA regions. Alternatively, it is possible that the isolated protein may be part of a multiprotein complex associated with the RNA. It is also possible that the proteins identified in association with the 5′ and 3′ UTR directly associate with only one region, and the folding of the RNA

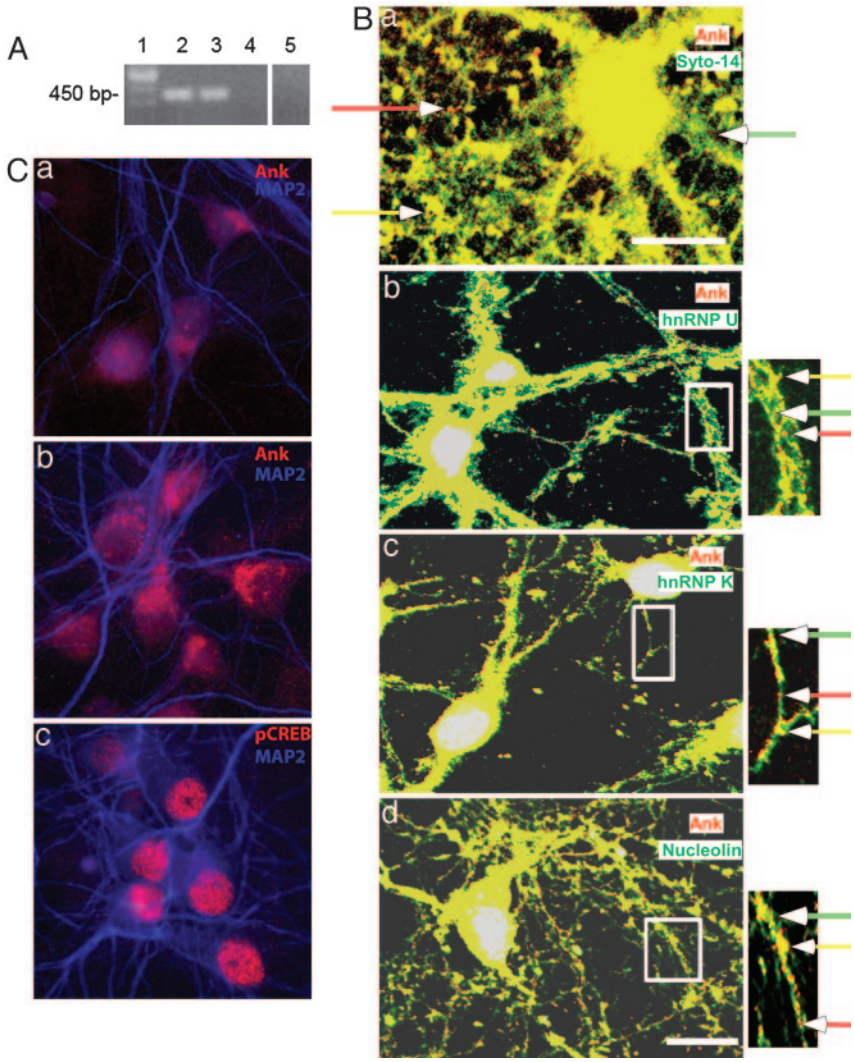

Fig. 4. Confirmation of *ank* mRNA association with selected RBPs and ank protein response to BDNF treatment. (*A*) Reverse transcription followed by nested PCR with *ank*-specific primers was performed on the samples immunoprecipitated with anti-nucleolin (lane 2), anti-hnRNP K (lane 3), and anti-GFP (lane 4). PCR products can be seen in nucleolin and hnRNP K lanes but not in the GFP control lane, indicating specific co-IP of *ank* mRNA with nucleolin and hnRNP K proteins. In lane 5, a bead-alone control is shown, where the lysate was run over the beads with no IP. (*B*) The immunocytochemical image (*Ba*) shows the coexistence of *ank* mRNA detected by ISH (visualized by streptavidin-594, in red) with Syto-14-stained RNA granules (green). Yellow indicates the presence of *ank* mRNA in RNA granules. Red, green, and yellow arrows represent the areas where *ank* mRNA, Syto-14 granules, and their overlap, respectively, are seen distinctly. The cellular coexistence of *ank* mRNA with various PAIR-identified RBPs is shown through the combination of *ank* mRNA ISH (red) with immunocytochemical localization of the RBPs (green) for hnRNP U (*Bb*), hnRNP K (*Bc*), and nucleolin (*Bd*). Yellow represents the cellular coexistence of the *ank* RNA with the various RBPs. The magnified portion of the image (*Insets* in *Bb–Bd*) shows *ank* mRNA (red arrow), RBP (green arrow), and their clear overlap (yellow arrow). (Scale bar, 10 μm.) (*C*) Primary hippocampal cultures were exposed to BNDF (50 ng/ml) for 6 h. The fluorescent signal derived from an anti-*ank* antibody (red) at time 0 (*Ca*) increased after the application of BDNF (*Cb*). Images were taken under the same exposure settings and modified to optimize the contrast in AXIOVISION with identical settings. The dendritic morphology was visualized by using an anti-microtubule-associated protein 2 antibody (blue). The immunocytochemical demonstration of phospho-cAMP response element-binding protein (pCREB) in the nucleus of most of the BDNF-treated cells shown in *Cc* serves as a positive control showing that BDNF was physiologically functional. pCREB fluorescence is apparent in $\approx$20% of the cells under normal conditions and, upon BDNF treatment, is increased to $>$95%.

orients the two regions spatially close enough to permit crosslinking with both. Consequently, there may be a direct and a proximity association. This may be why there are more similarities in RBPs associated with *ank* PNA 3 (in the 5′ UTR) and *ank* PNA 2 (in the 3′ UTR) than in those binding to *ank* PNA 1 and 2, which are offset by only a few bases in the 3′ UTR. This suggests an mRNA folding pattern that places the 5′ and 3′ UTR near each other and, more specifically, places the 5′ UTR in closer proximity to the 5′ portion of the 3′ UTR than the 3′ portion. This is in accord with the protein–mRNA complexes that are thought to control mRNA translation (35).

Two of the three PNAs were designed to anneal within the 3′ UTR, because the 3′ UTR of eukaryotic mRNA is known to contain cis elements involved in posttranscriptional regulation of gene expression. For example, located in the 3′ UTR of some mRNAs are AU-rich elements (AREs), sequences involved in regulating the decay of the transcript (36–38). The interaction of hnRNP A2 with AREs in some dendritically localized mRNAs (39, 40) is thought to be critical to the peripheral transport of these mRNAs (40, 41). *ank* mRNA, which can be dendritically localized (Fig. 4*B*), contains two AUUUA ARE sites within its 3′ UTR. hnRNP A2 was isolated in association with the 3′ UTR of *ank* mRNA and consequently may be involved in regulating the subcellular localization of *ank* mRNA. Given the *ank* protein involvement in bone remodeling, it is interesting to note that the overexpression of hnRNP A2 has been implicated as an autoantigen targeted by autoreactive T cells in the pathogenesis of rheumatoid arthritis (3).

Cortical cell stimulation by the growth factor BDNF results in the altering of the association of RBPs with *ank* mRNA in a position-dependent manner. This is direct evidence that RBP–mRNA interactions can be regulated by growth factor modulation. For example, AUF1, a RBP known to recognize and bind AREs (36, 37), was also identified in association with *ank* mRNA after BDNF treatment, as seen in Fig. 3 with all three PAIR–PNA probes. AUF1 binding to AREs has been shown to stabilize mRNAs and to increase their half life (42, 43). Because BDNF induces an increase in *ank* mRNA (data not shown) and protein levels (Fig. 4*C*), it is reasonable to speculate that this increase results in part from stabilization of *ank* mRNA through association with AUF1.

Nucleolin was repeatedly isolated in complex with *ank* mRNA at each of the three investigated regions. Because nucleolin is a ubiquitous nucleic acid-binding protein and was identified with each of the PNAs, we were concerned that nucleolin binding might be a nonspecific interaction. However, nucleolin binds the consensus sequence (U/G)CCCG(A/G), which is found in *ank* mRNA (nucleotides 314–319 and 1090–1095; GenBank accession no. AF393241), suggesting that nucleolin association with *ank* mRNA is specific. The ability to RT-PCR *ank* mRNA from a nucleolin IP further supports a specific association of *ank* RNA with nucleolin (Fig. 4*A*). Nucleolin was also observed in the vicinity of *ank* mRNA by using immunocytochemistry (Fig. 4*Bd*). Using PAIR–PNA

probes designed to other mRNAs that do not contain nucleolin cis-binding regions, little nucleolin binding was observed (data not shown).

Similar to nucleolin, both hnRNP K and hnRNP U were also assessed for their ability to associate with *ank* mRNA using immunocytochemical and/or IP methodologies (Fig. 4*B*). Image analysis shows coexistence of hnRNP U (Fig. 4) as well as hnRNP K with *ank* mRNA (Fig. 4*Bc*). hnRNP K was identified by PAIR in association with *ank* mRNA, specifically in the region of *ank* PNA 1 in the 3′ UTR under all tested conditions (Fig. 3). The inability to pharmacologically modulate this interaction suggests there is a basal level of *ank* RNA–hnRNP K complexes always present in cortical neurons. The specificity of the association was supported by the *ank* mRNA observed in hnRNP K IPs (Fig. 4*A*).

The detection of ribosomal proteins on *ank* mRNA after BDNF treatment suggests that the ribosomes load onto the *ank* mRNA in response to stimulation, perhaps to poise the *ank* RNA for a rapid increase in translation. This hypothesis is supported by the observed increase in *ank* protein in primary neuronal cells in culture that have been treated with BDNF (Fig. 4*C*). Fig. 4*Ca* shows immunohistochemically localized ank protein (red) under basal conditions, and Fig. 4*Cb* shows an increase in ank protein (red) after 6 h of BDNF treatment. Fig. 4*Cc* is a positive control showing that phospho-cAMP response element-binding protein is observed in the cells after BDNF treatment. Further, hnRNP A1, hnRNP C1/C2, and ribosomal protein L22 were found to associate with telomerase mRNA (44–46) and have also been found to increase under BDNF-stimulated conditions. Because telomerase dysfunction has been associated with the onset of rheumatoid arthritis (47), and also because the same RBPs bind to *ank* RNA, both of which are associated with arthritic physiology, it is tempting to speculate that these RBPs may be involved in coordinating aspects of normal bone physiology.

Comparison of data among several treatments is particularly striking, because DHPG stimulation and K^+ depolarization decreased the total number of RBPs that were isolated for each of the PNAs. The amount of nucleolin that binds to each of the three PNAs appears to be the same between treatments (Fig. 3), showing that the PNAs are able to anneal to *ank* RNA; consequently, the decrease in RBP binding during DHPG and K^+ treatments is a reflection of a change in the association of these RBPs to *ank* RNA. hnRNP D is also known as AUF1 and, as with the BDNF treatment, DHPG stimulates the association of AUF1 with *ank* mRNA. The physiological consequences of the overall decrease in RBP association with *ank* mRNA as modulated by K^+ or DHPG are unclear.

The high reproducibility of the associations of particular RBPs with *ank* mRNA and the confirmation of a subset of RBPs using biochemical and immunochemical approaches lead us to conclude that the PAIR technology provides a rapid and reliable way to detect a subset of proteins that interact with the target RNA *in vivo*. The data generated in this manuscript with three PNAs likely represent a subset of the RBPs that bind to *ank* RNA. Elucidation of the total RBP repertoire will require the synthesis and use of PAIR–PNAs that span the entire length of *ank* RNA. Although we have concentrated on identifying RBPs that bind to the UTRs of *ank* RNA, the PAIR methodology, using PAIR–PNAs directed to the coding region, will facilitate the characterization of RBPs that bind to the coding region of RNAs. It is anticipated that among the RBPs found with the PAIR technology will be proteins previously not known to bind to RNA. The cryptic RNA-binding domains of these RBPs will then be identified. This ability to characterize the RBPs that bind to RNAs *in vivo*, coupled with the ability to detect the RNAs that bind to any RBP *in situ* using the antibody-positioned RNA amplification procedure, should permit the detection and quantification of dynamic changes in RNA–RBP interactions that likely modulate many cellular physiological mechanisms.

Materials and Methods

Synthesis of the TP10–*ank*–PNA Compound. The incorporation of Bpa into PNA sequences sets no additional restrictions to conventional solid-phase peptide and PNA synthesis protocols. PNA oligomers with a general sequence Bpa-Cys-PNA-Lys-amide and the carrier peptide TP10 were synthesized from *tert*-butoxycarbonyl-protected building blocks on Applied Biosystems automated peptide synthesizer models 433A and 431A. The orthogonal amino group of ^{7}Lys in TP10 was specifically derivatized with 3-nitro-2-pyridinesulphenyl-labeled cysteine (Bachem). Molecular masses of PNA oligomers and the peptide were verified on a MALDI-TOF (Voyager-DE STR, Applied Biosystems) mass spectrometer. One micromolar of 3-nitro-2-pyridinesulphenyl-labeled peptide and free thiol containing PNA oligomer was conjugated in a mixture of 100 μl of DMSO/100 μl of dimethylformamide/300 μl of 0.1 M acetic buffer, pH 5.5. Reaction products were separated on a semi-preparative Discovery C18 columns, (25 cm × 10 mm, 5 μm, Sigma-Aldrich) HPLC column. The correct conjugate was determined by UV absorbance profile and MALDI-TOF mass spectrometry. Purity of the conjugates was >99%, as demonstrated by analytical HPLC.

Cortical Cultures. Cortical cell culture was performed as described for hippocampal cultures (48). Cortical cultures were maintained in NB for 7–22 days, cells were put through the PAIR procedure or treated with BDNF, high K^+, or DHPG. For these PAIR experiments, 50 ng/ml BDNF was added to the NB/B27 for 90 min, followed by addition of the PNA for 90 min, providing a total BDNF treatment time of 3 h. K^+ stimulation was executed by removing NB/B27 from the cells and replacing it with prewarmed MAPEX solution (145 mM NaCl/3 mM KCl/8 mM glucose/10 mM Hepes/3 mM $CaCl_2$/2.1 mM $MgCl_2$) for 5 min at 37°C in 5% CO_2, after which the solution was removed and replaced with prewarmed NB/B27. For DHPG-treated cells, a half-media change was performed with prewarmed NB/B27; after 30 min with these fresh media, DHPG was added for an additional 30 min to a final concentration of 20 mM.

PAIR Procedure. TP10–PNA conjugates were suspended in Hepes-buffered saline (HBS; 25 mM Hepes/0.75 mM Na_2HPO_4/70 mM NaCl), pH 7.4, at a concentration of 5 μM and stored at −20°C. Cortical cells in NB/B27 were incubated with 50 nM TP10–PNA for 90 min. The media were aspirated, and ice-cold HBS was quickly added. Before lysis, the cells were UV-irradiated for 2.5 min at a distance of 6 cm to crosslink the PNA and RBPs. The cells were then lysed in ice-cold TX-100 buffer (25 mM Hepes, pH 7.4/0.1% Triton X-100/300 mM NaCl/20 mM glycerophosphate/1.5 mM $MgCl_2$/1 mM DTT/200 nM Na_3VO_4/2 mM EDTA, pH 8.0/1 mM benzamidine/1 mM PMSF/2 μg/ml leupeptin/2 mg/ml aprotinin/1.4 mg/ml pepstatin). The cells were immediately harvested, and protein lysate was stored at −80°C until needed.

Isolation of PNA–RBP Complexes from Total Protein Lysate. An aliquot of total lysate was kept for gel analysis. The remaining lysate was rotated for 25 min at 37°C with 1 mg/ml RNase A followed by 1 h at room temperature with 100 mg of streptavidin magnetic beads (Pure Biotech, Middlesex, NJ) coupled to a biotinylated sense oligo to isolate the PNA–protein complex. The beads were washed twice with TX-100 buffer to remove any unbound material. The proteins were eluted by incubating at 50°C for 20 min with 30 μl (100 μl for precipitation) of prewarmed salt-free TX-100 buffer. PAGE was performed by using NuPAGE 10% Bis-Tris Gels (Invitrogen). Gels were Coomassie-stained and destained using standard procedures. Protein bands enriched in the bound protein lane were extracted from the gel, and slices were stored in 1–2% acetic acid at −20°C for mass spectrometry. As an alternative to the gel band isolations, the eluted protein preparation can be precip-

itated by using the chloroform–methanol precipitation method (49) and analyzed *en masse*.

Mass Spectrometry. Protein bands from Coomassie-stained gels or the total chloroform–methanol precipitate were digested with trypsin. The digested peptides were loaded to C18 column, separated with nanoLC [Dionex/LC Packings (Amsterdam) Famous/Switch/Ultimate 2D nanoLC]. The eluted peptides from 60-min gradient were sequenced with nanospray/Qstar-XL (Applied Biosystems) (50). The raw data were searched with MASCOT (Matrix Science, Boston) against the National Center for Biotechnology Information database.

Fluorescence Imaging of the CPP–PNA Permeation of Cortical Neurons. Oregon green 488-labeled sense oligo (480 ng) was heated to 70°C for 5 min and slowly cooled to 40°C, at which point 120 ng of *ank* PNA 1 was added in Hepes-buffered saline and slowly cooled to room temperature. The annealed fluorescently labeled oligonucleotide–*ank* PNA 1 was incubated with cortical neurons for 90 min in NB/B27. After washing, the coverslips were mounted with DAPI–Vectashield and the fluorescence visualized.

IP of mRNA–Protein Complexes. Rat cortical neurons were harvested in polysome lysis buffer [100 mM KCl/5 mM $MgCl_2$/10 mM Hepes, pH 7.0/0.5% Nonidet P-40/1 mM DTT/100 units/ml RNasin Ribonuclease Inhibitor (Promega)/2 mM Vanadyl Ribonucleoside Complexes Solution (BioChemica, Melbourne, FL)/25 μl/ml Protease Inhibitor Mixture for Mammalian Tissues (Sigma)]. Lysate, handled at 4°C, was centrifuged at 16,000 $\times g$ for 15 min, precleared twice for 1 h with Protein A Agarose (Invitrogen), and aliquoted for IPs. Rabbit polyclonal antibodies (Santa Cruz Biotechnology) antinucleolin/C23 (H-250), anti-hnRNP K (H-300), and anti-GFP (FL) were added at 10 μg/1 ml of lysate ($\approx$1 mg of protein). One aliquot of cellular lysate, from which the antibody was omitted, was processed through the protocol as a control for nonspecific binding to protein A–agarose beads (bead control). Samples were rotated at 4°C overnight. Protein A agarose beads (50 μl) were added to each sample and rotated for 4 h at 4°C. The beads were pelleted and washed four times with 0.5 ml of lysis buffer for 5 min each and another four times with lysis buffer containing 1 M urea. The beads were resuspended in 100 μl of lysis buffer containing 0.1% SDS and 30 μg of proteinase K and incubated at 50°C for 30 min, followed by phenol–chloroform extraction and ethanol precipitation. The pellet was resuspended in 13 μl of reverse transcription (RT) mix containing dNTPs (500 mM each) and 100 nM primer for *ank* mRNA (3′ *ANK*PCR2: TGTTGATTCTTAGGAGAC). RT was done by using SuperScript III Reverse Transcriptase (Invitrogen) and used as a template for PCR. PCR was done by using AccuPrime SuperMix I (Invitrogen) with 250 nM primers 5′*ANK*PCR1 (CTCATCTCACTGGATGGT) and 3′*ANK*PCR2 (TGT TGATTCTTAGGAGAC) for 25 cycles. This first-round PCR reaction was used as a template for a second round of PCR with primers 5′*ANK*PCR1 and 3′*ANK*PCR1 (GCCTCTTTCATAACCAAG) for 30–35 cycles.

Immunocytochemical Detection of Proteins in Cortical Neurons and RNA Granule Staining. The cells were fixed in 4% paraformaldehyde for 5 min followed by washes with PBS/0.12 M sucrose and PBS/5 mM $MgCl_2$ three times each for 5 min. After blocking, the cells were incubated overnight at room temperature with one of the following primary antibodies obtained from Santa Cruz Biotechnology: antinucleolin (C-23, 1:100), anti-hnRPN K (N-20, 1:50), anti-hnRPN U (C-15, 1:100), diluted in blocking solution. Secondary antibody association with the primary antibodies was accomplished by using donkey anti-goat antibody labeled with Alexa Fluor 488 (Molecular Probes). Staining for RNA granules was performed by using Syto-14 dye (34). Fluorescence was imaged with confocal microscopy.

ISH Detection of *ank* mRNA. The following primers that anneal to different regions of the *ank* mRNA were synthesized with 5′-biotin to facilitate subsequent visualization: *ank* nucleotides 361–409, 829–878, 1230–1276, 1915–1965, and 2054–2100.

The combined immunocytochemical/ISH protocol used (51) an equimolar mixture of *ank* primers hybridized at a concentration of 20 ng/μl primer at 42°C for 18 h. After washing, the sections were air-dried, mounted, and visualized using fluorescently labeled Streptavidin-350 or -594. The images were captured by using Olympus (Melville, NY) FluoView Confocal Microscope.

We thank Margie Maronski for culturing of the primary rat cortical neurons. This work was funded in part by National Institutes of Health Grants MH58561 and AG9900 (to J.E.), the Swedish Science Foundation Grants Med and NT, and European Community Grant QLRT-2001-01989.

1. Maquat, L. E. & Carmichael, G. G. (2001) *Cell* **104,** 173–176.
2. Musunuru, K. & Darnell, R. B. (2001) *Annu. Rev. Neurosci.* **24,** 239–262.
3. Fritsch, R., Eselbock, D., Skriner, K., Jahn-Schmid, B., Scheinecker, C., Bohle, B., Tohidast-Akrad, M., Hayer, S., Neumuller, J., Pinol-Roma, S., *et al.* (2002) *J. Immunol.* **169,** 1068–1076.
4. Pellizzoni, L., Kataoka, N., Charroux, B. & Dreyfuss, G. (1998) *Cell* **95,** 615–624.
5. Turner, G., Webb, T., Wake, S. & Robinson, H. (1996) *Am. J. Med. Genet.* **64,** 196–197.
6. Tenenbaum, S. A., Carson, C. C., Lager, P. J. & Keene, J. D. (2000) *Proc. Natl. Acad. Sci. USA* **97,** 14085–14090.
7. Brown, V., Jin, P., Ceman, S., Darnell, J. C., O'Donnell, W. T., Tenenbaum, S. A., Jin, X., Feng, Y., Wilkinson, K. D., Keene, J. D., *et al.* (2001) *Cell* **107,** 477–487.
8. Ule, J., Jensen, K. B., Ruggiu, M., Mele, A., Ule, A. & Darnell, R. B. (2003) *Science* **302,** 1212–1215.
9. Miyashiro, K. Y., Beckel-Mitchener, A., Purk, T. P., Becker, K. G., Barret, T., Liu, L., Carbonetto, S., Weiler, I. J., Greenough, W. T. & Eberwine, J. (2003) *Neuron* **37,** 417–431.
10. Nielsen, P. E., Egholm, M., Berg, R. H. & Buchardt, O. (1991) *Science* **254,** 1497–1500.
11. Xi, C., Balberg, M., Boppart, S. A. & Raskin, L. (2003) *Appl. Environ. Microbiol.* **69,** 5673–5678.
12. Egholm, M., Buchardt, O., Christensen, L., Behrens, C., Freier, S. M., Driver, D. A., Berg, R. H., Kim, S. K., Norden, B. & Nielsen, P. E. (1993) *Nature* **365,** 566–568.
13. Zaffaroni, N., Villa, R., Pennati, M. & Folini, M. (2003) *Mini. Rev. Med. Chem.* **3,** 51–60.
14. Nielsen, P. E. (2001) *Curr. Opin. Biotechnol.* **12,** 16–20.
15. Brandt, O., Feldner, J., Stephan, A., Schroder, M., Schnolzer, M., Arlinghaus, H. F., Hoheisel, J. D. & Jacob, A. (2003) *Nucleic Acids Res.* **31,** e119.
16. Knudsen, H. & Nielsen, P. E. (1996) *Nucleic Acids Res.* **24,** 494–500.
17. Lewis, M. R., Jia, F., Gallazzi, F., Wang, Y., Zhang, J., Shenoy, N., Lever, S. Z. & Hannink, M. (2002) *Bioconjug. Chem.* **13,** 1176–1180.
18. Nielsen, P. E. (2000) *Curr. Opin. Mol. Ther.* **2,** 282–287.
19. Ray, A. & Norden, B. (2000) *FASEB J.* **14,** 1041–1060.
20. Cutrona, G., Carpaneto, E. M., Ulivi, M., Roncella, S., Landt, O., Ferrarini, M. & Boffa, L. C. (2000) *Nat. Biotechnol.* **18,** 300–303.
21. Pooga, M., Hallbrink, M., Zorko, M. & Langel, U. (1998) *FASEB J.* **12,** 67–77.
22. Hallbrink, M., Floren, A., Elmquist, A., Pooga, M., Bartfai, T. & Langel, U. (2001) *Biochim. Biophys. Acta* **1515,** 101–109.
23. Pooga, M., Soomets, U., Hallbrink, M., Valkna, A., Saar, K., Rezaei, K., Kahl, U., Hao, J. X., Xu, X. J., Wiesenfeld-Hallin, Z., *et al.* (1998) *Nat. Biotechnol.* **16,** 857–861.
24. Soomets, U., Lindgren, M., Gallet, X., Hallbrink, M., Elmquist, A., Balaspiri, L., Zorko, M., Pooga, M., Brasseur, R. & Langel, U. (2000) *Biochim. Biophys. Acta* **1467,** 165–176.
25. Ho, A. M., Johnson, M. D. & Kingsley, D. M. (2000) *Science* **289,** 265–270.
26. Eberwine, J., Belt, B., Kacharmina, J. E. & Miyashiro, K. (2002) *Neurochem. Res.* **27,** 1065–1077.
27. Behlen, L. S., Sampson, J. R. & Uhlenbeck, O. C. (1992) *Nucleic Acids Res.* **20,** 4055–4059.
28. Pino, I., Pio, R., Toledo, G., Zabalegui, N., Vicent, S., Rey, N., Lozano, M. D., Torre, W., Garcia-Foncillas, J. & Montuenga, L. M. (2003) *Lung Cancer* **41,** 131–143.
29. Wilk, H. E., Werr, H., Friedrich, D., Kiltz, H. H. & Schafer, K. P. (1985) *Eur. J. Biochem.* **146,** 71–81.
30. Ma, A. S., Moran-Jones, K., Shan, J., Munro, T. P., Snee, M. J., Hoek, K. S. & Smith, R. (2002) *J. Biol. Chem.* **277,** 18010–18020.
31. Weiler, I. J. & Greenough, W. T. (1993) *Proc. Natl. Acad. Sci. USA* **90,** 7168–7171.
32. Kacharmina, J. E., Job, C., Crino, P. & Eberwine, J. (2000) *Proc. Natl. Acad. Sci. USA* **97,** 11545–11550.
33. Tongiorgi, E., Righi, M. & Cattaneo, A. (1997) *J. Neurosci.* **17,** 9492–9505.
34. Knowles, R. B., Sabry, J. H., Martone, M. E., Deerinck, T. J., Ellisman, M. H., Bassell, G. J. & Kosik, K. S. (1996) *J. Neurosci.* **16,** 7812–7820.
35. Cao, Q. & Richter, J. D. (2002) *EMBO J.* **21,** 3852–3862.
36. Guhaniyogi, J. & Brewer, G. (2001) *Gene* **265,** 11–23.
37. Wilusz, C. J., Wormington, M. & Peltz, S. W. (2001) *Nat. Rev. Mol. Cell Biol.* **2,** 237–246.
38. Gillis, P. & Malter, J. S. (1991) *J. Biol. Chem.* **266,** 3172–3177.
39. Ainger, K., Avossa, D., Diana, A. S., Barry, C., Barbarese, E. & Carson, J. H. (1997) *J. Cell Biol.* **138,** 1077–1087.
40. Munro, T. P., Magee, R. J., Kidd, G. J., Carson, J. H., Barbarese, E., Smith, L. M. & Smith, R. (1999) *J. Biol. Chem.* **274,** 34389–34395.
41. Shan, J., Munro, T. P., Barbarese, E., Carson, J. H. & Smith, R. (2003) *J. Neurosci.* **23,** 8859–8866.
42. Xu, N., Chen, C. Y. & Shyu, A. B. (2001) *Mol. Cell. Biol.* **21,** 6960–6971.
43. Loflin, P., Chen, C. Y. & Shyu, A. B. (1999) *Genes Dev.* **13,** 1884–1897.
44. Ford, L. P., Suh, J. M., Wright, W. E. & Shay, J. W. (2000) *Mol. Cell. Biol.* **20,** 9084–9091.
45. Le, S., Sternglanz, R. & Greider, C. W. (2000) *Mol. Biol. Cell* **11,** 999–1010.
46. Dallaire, F., Dupuis, S., Fiset, S. & Chabot, B. (2000) *J. Biol. Chem.* **275,** 14509–14516.
47. Yudoh, K. & Matsuno, H. (2001) *Drugs Today (Barcelona)* **37,** 595–606.
48. Buchhalter, J. R. & Dichter, M. A. (1991) *Brain Res. Bull.* **26,** 333–338.
49. Wessel, D. & Flugge, U. I. (1984) *Anal. Biochem.* **138,** 141–143.
50. Jackson, C. L. (2004) *Nat. Cell Biol.* **6,** 379–380.
51. Prakash, N., Fehr, S., Mohr, E. & Richter, D. (1997) *Eur. J. Neurosci.* **9,** 523–532.